Magnetic Resonance Techniques for Fat Quantification in Obesity

Houchun Harry Hu
Radiology, Children's Hospital Los Angeles, Los Angeles, California, USA
E-mail: hhu@chla.usc.edu, houchunh@usc.edu Tel: +1-323-361-2688

Abstract— **As the prevalence of obesity and its comorbidities continue to rise in the United States and worldwide, robust imaging techniques and accurate post-processing strategies are critically needed to accurately quantify the distribution of fat in the human body. Magnetic resonance imaging and spectroscopy provide a wide array of sensitive methods to assess and characterize fat in storage locations such as white adipose tissue depots and "high-health-risk" ectopic sites such as organs and muscles. Quantitative fat measurements provide useful information to investigators in preventive medicine who monitor the efficacy of dietary, exercise, and surgical interventions to combat weight gain and obesity in longitudinal studies. They are also useful to clinicians who study the implications of steatosis and the pathophysiology of fat. The primary aim of this paper is to provide a technical review of state-of-the-art proton magnetic resonance methods in human body fat quantification. The paper will emphasize the fundamental principles with which several magnetic resonance techniques differentiate lean (water-dominant) and fatty (fat-dominant) tissues and illustrate with examples how each method can be appropriately used for fat quantification. The paper will also briefly summarize post-processing procedures that are currently in practice for extracting quantitative fat endpoints, such as adipose tissue depot volume and percent fat content in organs. Lastly, given its increased attention in recent literature, the paper will discuss progress in the imaging of human brown adipose tissue.**

I. Introduction: "Fat is No Longer Just Fat"

Consider the following health questions in the context of human obesity. How much fat is too much fat in the body? How is fat accumulation in the human body influenced by aging, gender, ethnicity, diet, and exercise? Does it matter where fat is stored in the human body? Related, are certain locations of fat deposition associated more adversely with risks for diseases like cancer, diabetes, and cardiovascular abnormalities? Currently, imaging modalities like computed tomography and magnetic resonance that can provides high resolution anatomical visualizations within the body and quantify fat distributions play a critical role in epidemiological studies that aim to answer these questions.

The prevalence of obesity in children, adolescents, and adults continues to rise in the United States and worldwide in developed countries [1-6]. Childhood obesity is of particular concern, as obese children are at a much greater chance of becoming obese adults with lifelong health risks [7]. The capability to accurately assess fat distributions in white adipose tissue depots and organs within the human body is useful to investigators studying therapeutic and preventive measures against weight gain, obesity, and the patho-physiology of fat. Whereas fat is typically stored in the form of white adipose tissue in the subcutaneous depot, it has been well established that the deposition of fat in the intra-abdominal (visceral) depot and further accumulation of fat in ectopic sites such as the liver, pancreas, heart, and skeletal muscles are particularly detrimental to health and play a critical role in determining one's metabolic profile and risk for disease [8-15]. Thus, the development of accurate, reliable, and rapid data acquisition and post-processing techniques that can quantify adipose tissue volumes and ectopic fat contents remains a vibrant area of ongoing research. Magnetic resonance imaging (MRI) and spectroscopy (MRS) methods are non-invasive, utilizes no ionizing radiation, provides tomographic 3D visualization of the anatomy, has immense flexibility in tissue contrast mechanisms, is safely repeatable across longitudinal studies without restrictions, and is applicable to cohorts of all ages, particularly in children and adolescents.

This paper will review several popular proton MR techniques for quantitative fat imaging. It begins with a description of MR principles and is intended to provide the reader with basic knowledge and familiarize them with terminology. Next, emphasis is placed on approaches such as traditional T_1-weighted imaging, frequency-selective imaging, single-voxel MRS, and state-of-the-art chemical-shift-encoded water-fat techniques. Post-processing computations and image segmentation procedures for extracting quantitative fat endpoints will also be summarized. Lastly, the paper will also allude to recent progress in the imaging of human brown adipose tissue and its implications in obesity research.

II. Background and Motivation

For a majority of MR applications, the composite signal is assumed to come primarily from a two-component model: hydrogen protons of free water in tissues and fat (triglyceride, free fatty acid) molecules. While other protons exist in macromolecules, minerals, and proteins, they are usually not visible with conventional MR hardware. When an object is placed inside a magnetic field of strength B_0, a longitudinal magnetization from the visible proton ensemble is created. The magnetization establishes resonance at a specific Larmor frequency proportional to the B_0 field strength. During a scan, a train of radiofrequency (RF) pulses is applied every TR

(repetition time) to gather data via a pulse sequence. The pulses are tuned to the Larmor frequency, have a certain bandwidth, and repeatedly excite the longitudinal magnetization into the transverse plane for signal detection. After each excitation, an echo of the transverse magnetization is acquired by coil receivers at a time specified by TE (echo time). After each successive RF excitation, two processes occur. First, the perturbed longitudinal magnetization recovers towards its original state prior to RF excitation. The rate of recovery is called T_1. Second, the transverse magnetization loses signal coherence and decays at a rate called T_2. T_1 and T_2 values are intrinsic tissue properties and serve as the predominant basis of signal contrast in clinical MR [16, 17].

It is worth noting that at human whole-body B_0 field strengths of 1.5 Tesla (T) and 3T, the proton Larmor frequency is on the order of 64 and 128MHz, respectively. However, as it will be described later, there is in fact a slight difference in resonance frequency between water and fat protons, and it is this difference, albeit a very small one on the order of 10^2 Hz, that underpins several sensitive MR water-fat detection methods. Overall, one of the goals of any quantitative fat imaging then is to identify mechanisms that can highlight from the acquired composite MR signal the desired component. In this context, it is fat.

It is important to mention at this point that the MR signal intensity generally has arbitrary units, and is influenced by a host of non-linear factors including tissue-specific proton density and relaxation rates (T_1 and T_2) and pulse sequence timings (TR and TE) and the RF excitation flip angle. Furthermore, given fixed imaging parameters, the resulting signal intensity can vary significantly across MR platforms and manufacturers. In quantitative MR of fat, the key then is to relate the measured signal to a more objective metric that can facilitate meaningful comparisons. In other words, an imaging biomarker is needed. An imaging biomarker is an objective indicator of a biological, pathological, or pathogenic process. The accuracy of a biomarker is the correctness with which it compares against a reference "ground truth" measurement, and this can be assessed with receiver operating curves and true/false positives/negatives if the metric is dichotomous or with correlation and regression if the measure is continuous or ordinal. Precision refers to the consistency (and variability) of the biomarkers. In contrast to accuracy, no reference standard is needed in assessing precision. Precision is affected by technical components including repeatability (within a site, within examinations, between examinations), reproducibility (between sites, between manufacturers and variants in B_0 field strength and platforms), and robustness (invariance to changes in pulse sequence parameters, operator). Precision is also affected by biological components, including temporal variability (within day, between days, in response to physiological changes) and spatial variability in cross-sectional and longitudinal studies. While accuracy is critical in single-site studies, precision is equally important when considering multi-site studies. Standardization efforts are needed to properly integrate a biomarker into research trials and routine clinical practice.

As summarized in Fig. 1, in the MR literature, the most commonly reported fat measurements for white adipose tissue depots are either volume (ml, L) or mass (g, kg), the latter of which is simply converted from the former by scaling with the mass density of fat. As discussed in the following section, the identification and segmentation of triglyceride-rich white adipose tissue depots can be achieved with strategies that highlight the signal intensity of fat in contrast to surrounding lean tissues and organs. For diffuse ectopic fat measurements, the ratio of water and fat signals, the fat signal fraction, is commonly reported. If the water and fat signals are additionally corrected for confounding factors such as T_1 and T_2 relaxation [18], then the net ratio reflects the proton density fat fraction, or PDFF. Fig. 1 also illustrates the "take-home-message" from the remainder of this paper. Proton MR techniques that can appropriately quantify white adipose tissue depots and ectopic fat content are listed below the dashed line.

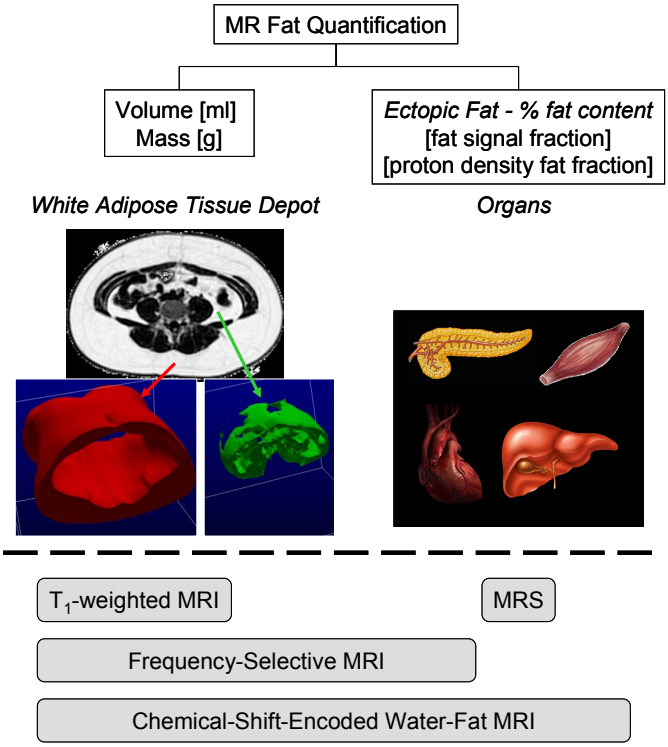

Fig. 1 Typical fat quantification endpoints in MR include volume or mass for white adipose tissue depots (red: subcutaneous, green: intra-abdominal), which are comprised primarily of fat, and fat signal fraction in ectopic sites of diffuse fat accumulation such as the pancreas, skeletal muscles, heart, and liver. When corrected for various confounding factors such as signal relaxation, noise bias, RF excitation flip angle, and the complex fat spectrum, the ratio is referred to as the proton density fat fraction as it more accurately approximates the true underlying tissue fat concentration. Listed below the dashed line are the current proton MR methods that can appropriately quantify the endpoints. While T_1-weighted MRI and MRS can only quantify adipose tissue volume and organ fat signal fraction, respectively, both frequency-selective and chemical-shift-encoded water-fat MRI have capabilities to quantify both endpoints, with the latter being more commonly used.

III. T_1- AND T_2- WEIGHTED APPROACHES

The simplest approach to differentiate fat in white adipose tissue depots from other water-dominant anatomical structures is to exploit the natural differences in the T_1 and T_2 relaxation rates between water and fat protons. The T_1 of fat is one of the shortest amongst tissues in vivo. This indicates a very rapid recovery of its longitudinal magnetization between successive RF excitations. Therefore, by using a T_1-weighted sequence, strong tissue contrast can be achieved between short-T_1 fat tissues and muscles and organs with longer T_1 values, as illustrated in Fig. 2. Bright fat can thus often be easily identified and delineated from darker structures by simple image processing (e.g. bias-field correction, histogram thresholding). T_1-weighted sequences are very common in clinical MRI and are the "tried–and–true" workhorse tool for rapidly assessing abdominal subcutaneous and visceral white adipose tissue distributions (Fig. 3) as well as whole-body adiposity and have served as the basis for many semi-automated and automated segmentation techniques in the literature [19-26]. Additionally, the explicit computation of T_1 values on a voxel-wise basis has also been employed to improve white adipose tissue depot identification and facilitate automated image segmentation [27].

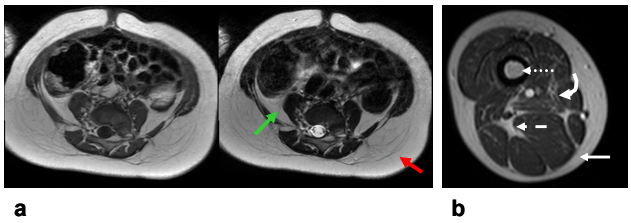

Fig. 2 (a) Complementary T_1- (left) and T_2-weighted (right) transverse images at the level of the umbilicus in a 9-months-old girl. Note that subcutaneous (red arrow) and visceral adipose (green arrow) tissue depots are represented by bright signal intensities in both types of signal contrast. (b) T1-weighted transverse image of the thigh in an eight-year-old boy with Duchenne Muscular Dystrophy. Note the subcutaneous (solid arrow) and intermuscular adipose tissues (dashed arrow), and the bone marrow (dotted arrow), both of which appear bright due to their fatty composition. Note also the diffuse appearance of fat infiltration into various muscle groups (curved arrow).

The T_2 of fat is neither the shortest nor the longest. Nonetheless, fat appears relatively bright, but is often not the brightest structure on conventional T_2-weighted images (see Fig. 2). In comparison to T_1-weighted pulse sequences, T_2-weighted are typically longer in duration and are thus rarely chosen for the sole purpose of white adipose tissue quantification. Both T_1-weighted and T_2-weighted images are not appropriate for estimating ectopic fat content because the acquired signal within each image voxel represents the sum of signal contributions from both water and fat protons and the individual component signals are not known. However, while these strategies are only appropriate for quantifying white adipose tissue depots, they are often used clinically in a qualitative manner to visually determine the potential presence (or absence) of fat in pathological conditions, such as in the muscle [28] and heart [29, 30].

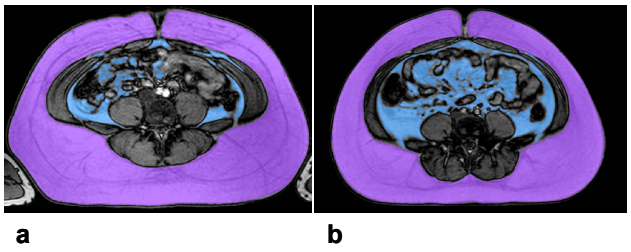

Fig. 3 Segmented T_1-weighted transverse images at the umbilicus in two females, both 22 years of age and with similar body-mass-indices (a: 31.4 kg/m^2) versus (b: 32.3 kg/m^2). Subject in (a) is African-American. Subject in (b) is Hispanic. Note the evident difference in visceral (blue) adipose tissue volumes, despite somewhat similar amounts of subcutaneous adipose tissue (purple). Elucidating the differences in gender and age-related variations in body adiposity and the biological causes of such differences is a strong area of research in obesity. Segmentations were performed with SliceOmatic software (Tomovision, Inc.).

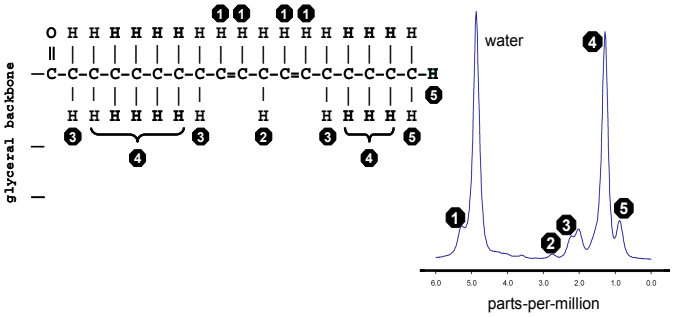

Fig. 4 Unlike water, which has a single proton resonance in the frequency domain, fat is characterized by a more complex spectrum with multiple peaks. The five most common resonances are illustrated on the right. Depending on the number of carbon-carbon double bonds in the triglyceride, a measure of unsaturation, as well as the length of the triglyceride chains, the amplitudes (area under the curve) of peaks 1 through 4 peaks can slightly vary. Illustration courtesy of Gavin Hamilton, Ph.D. from the University of California, San Diego.

IV. WATER-FAT CHEMICAL-SHIFT

Before proceeding further, it is appropriate at this point to briefly discuss the phenomenon of chemical-shift in proton magnetic resonance techniques. Water is a symmetrical molecule (H_2O) with two identical protons, and thus exhibits a single Larmor frequency, or proton resonance peak in the frequency domain. In contrast, a typical triglyceride (fat) molecule is much more complex and contains three possibly different fatty acid chains (one of which is shown in Fig. 4). Consequently, there are several proton moieties in fat [31, 32], including among others, the predominant (-CH_2-) methylene group, the terminal (-CH_3) methyl group, and the (-CH=CH-) olefinic group. Each of these proton moieties experience a slightly different local magnetic field due to electron shielding from its chemical neighbors along the fatty acid carbon chain, and thus lead to distinct proton resonance peaks in the

frequency domain that are chemically-shifted from each other and that of water (see Fig. 4). Historically, the chemical shift separation is measured in units of ppm: parts-per-million, and is displayed on an inverted horizontal axis. The nominal frequency separation is dependent on the magnetic B_0 field strength. For water and the predominant methylene peak of fat, it is approximately 210Hz at 1.5T, and 420Hz at 3T.

V. Single-Voxel MR Spectroscopy

Single-voxel proton spectroscopy has long been considered the gold-standard for ectopic fat quantification as it provides the most direct and sensitive approach to discriminate water and fat proton component signals in MR. The technique has been widely investigated, refined, and adopted for routine use in assessing liver, heart, pancreas, and skeletal muscles fat content [33-44]. In contrast to MR imaging, localized single-voxel MRS does not provide anatomical information with a grayscale image. Instead, it yields a detailed and accurate frequency spectrum within an interrogated voxel, which provides an intuitive visualization of the presence and quantity of water, fat and other proton moieties. The relative area under each spectral resonance peak is directly proportional to the concentration of a particular proton specie (number of protons) within the sampled voxel. Although the spectrum can be theoretically modeled as a series of delta functions, in reality, line broadening occurs due to T_2 relaxation and inhomogeneities within the B_0 field.

In practice, the acquisition and analysis of MRS data requires some expertise and experience, and can be performed using software available commercially on the MR system or offline with dedicated packages such as jMRUI [45] and LCModel [46]. Regardless of the approach, MRS analysis requires user interaction, as automated, robust, and reliable strategies are not yet available. This remains an unmet challenge in data processing. Typical steps includes noise filtering, baseline and phase correction, and modeling and fitting each individual resonance with a single or multiple weighted overlapping Gaussian or Lorenzian distributions. The fitted curves are subsequently integrated to estimate the area under each peak. The resultant fat signal fraction is then computed as the sum of the areas under all of the fat peaks divided by the sum of the water and fat peak areas. If additional T_1 and T_2 corrections are performed on the individual resonances, then the fat signal fraction better approximates the proton density fat fraction, which has been shown to accurately reflect the true underlying tissue fat content [47]. Fig. 5 illustrates two examples in the liver.

It is worth mentioning that presently MRS remains the only imaging method that can uniquely differentiate between ectopic intra- and extra- myocellular lipids in skeletal muscle [33, 48]. Whereas IMCL consists of spherical fat droplets and provide energy to muscles metabolism, EMCL lipids are arranged in parallel plates and exhibit characteristics similar to adipose tissue. Magnetic susceptibility causes a very minute difference in the Larmor frequencies of the $-CH_2-$ resonances between IMCL and EMCL [33, 48, 49], and maximal difference occurs when the muscle fibers and the B_0 magnetic field are parallel. In obesity and metabolism research, it has been shown that IMCL levels in particular can fluctuate with insulin sensitivity, physical activity, diet, and pharmacological effects. Specifically, in obese, sedentary, and diabetic patients, high IMCL levels [50] and low insulin sensitivity are characteristic negative indicators of metabolic health [51, 52]. Interestingly however, in athletes, a paradox exists where both high IMCL and insulin sensitivity are observed [53-55].

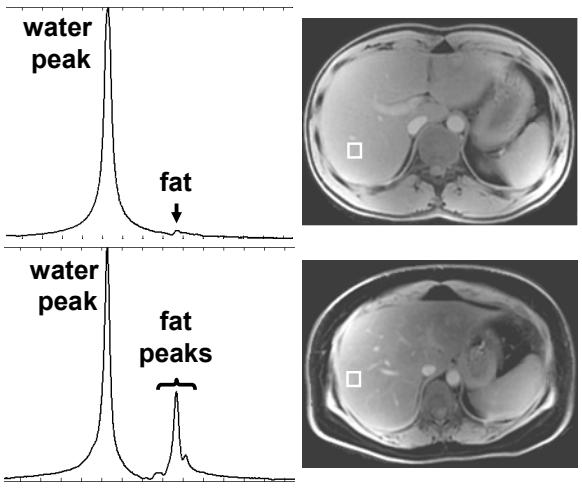

Fig. 5 Example of single-voxel proton MRS of the liver in two subjects, one with a lean liver (top), the other with a fatty liver (bottom). Anatomical images are shown on the left for reference, and the white boxes denote the location of the sampled MRS voxels. Note that the difference in hepatic fat content is indistinguishable on the anatomical images, but is strongly evident on the MRS spectra. The fat signal fractions were 3% (top) and 23% (bottom), respectively. Note line broadening in the spectra.

VI. Frequency-Selective MRI

The chemical shift phenomenon between water and fat can be extended to MR imaging methods [56, 57]. Since data acquisition in MRI fundamentally involves frequency-tuned RF pulses that excite a measurable proton magnetization into the transverse plane prior to data acquisition, the feasibility of selectively exciting only fat protons [36, 58, 59], or conversely suppressing the water signal with a preceding RF preparation pulse [60, 61], has been explored as a complementary method for quantifying subcutaneous, visceral, and intermuscular white adipose tissue volumes. The primary motivation behind frequency-selective strategies is similar to that of the aforementioned T_1-weighted approaches, where a strong signal contrast is desired between water-dominant and fat-dominant tissues such that post-processing segmentation can be easily facilitated. In the present case, stronger tissue contrast can be achieved by selectively suppressing or exciting one of the two (water, fat) components.

Fig. 6 schematically illustrates water-selective and fat-selective imaging in the form of RF suppression. It should be realized that intuitively, a complementary pair of frequency-selective and non-frequency-selective images with otherwise

identical imaging parameters can highlight the presence of ectopic fat within each imaging voxel. Consider for example a voxel containing both water and fat signals. Signal intensity from a non-frequency-selective scan reflects the sum of both water and fat components. However, if a complementary fat-selective excitation scan is performed, the resultant signal intensty is equal only the fat component. In this respect, a fat signal fraction can be approximated. It then becomes evident that for a voxel containing only fat, the signal intensities between the pair of should be identical (fat signal fraction = 100%). Conversely, for a particular voxel containing only water, the fat-selective image will have ideally an intensity of zero (fat signal fraction = 0%), or in reality, just noise.

Many frequency-selective strategies adopt a simplified spectral model of fat, where only the predominant methylene peak and other fat peaks in close proximity to it are considered (peak 3 through 5 in Fig. 4). Consequently, it is recognized that the computed fat signal fraction reflects only contributions from these resonances and is not expected to be in perfect agreement, though likely correlated, when compared against MRS or other techniques that do account for more peaks in the fat spectrum, in particular the olefinic resonance.

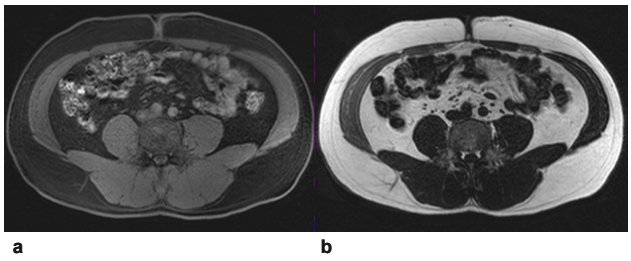

Fig. 6 A demonstration of (a) fat-suppressed and (b) water-suppressed transverse images. Note in (a) near the bottom of the image where the subcutaneous adipose tissue appears in very light shades of gray, indicative of the fact that not all of the resident fat signals have been suppressed. One reason for this is the olenific fat resonance that is located in proximity to the water spectral peak and is typically not RF-suppressed in frequency-selective MRI.

VII. Chemical-Shift-Encoded Water-Fat MRI

Chemical-shift-encoded water-fat MRI, heretofore referred to simply as WFI, combines to a certain extent the sensitive detection capabilities of MRS with the benefits of anatomical imaging [62-65] to facilitate combined quantification of both white adipose tissue depots and ectopic fat content from a single MRI scan. WFI consists of a family of MRI techniques that have been continuously developed and refined since 1984, when W.T. Dixon first introduced the concept "simple spectroscopic imaging" [66]. By selecting two appropriate echo times for data acquisition where water and fat signal vectors accrue progressive phases with respect to one another as a consequence of their chemical shift difference, Dixon demonstrated that separate water and fat images can be subsequently reconstructed by simple mathematics. By reconstructing separated water and fat images, a fat signal fraction map (fat:water ratio) can then be computed.

In contrast to single-voxel MRS where no parameters about the frequency spectrum is assumed, WFI can be considered as a subset, where a crucial feature is that the water and fat chemical-shift resonances and their relative amplitudes are assumed known and modeled *a priori* into the underlying signal equation and reconstruction algorithm. In contrast to frequency-selective methods, WFI strategies do not employ frequency-tuned RF pulses for targeted signal excitation or suppression of water or fat. Rather, unsuppressed water and fat signals are both acquired by data coil receivers at strategically chosen echo times. Subsequently, elegant mathematical algorithms are used to solve for the individual unknown water and fat signal components on a voxel-wise basis, based on the assumed spectral model, numerical assumptions, and parameter constraints [67-71].

Recent advances in WFI have also led to major efforts in improving the accuracy and precision of the computed fat signal fraction and its reflection of the true underlying tissue PDFF. A plethora of works have identified and addressed a variety of signal confounding factors, including T_1 and T_2 relaxation, noise bias, and systematic phase errors [72-74] that can erroneously impact the estimation of PDFF. Additionally, numerous clinical and research studies have rigorously validated the utility of WFI in quantifying both white adipose tissue depots [75] as well as ectopic fat in the liver [76-79], heart [80], and skeletal muscles [81].

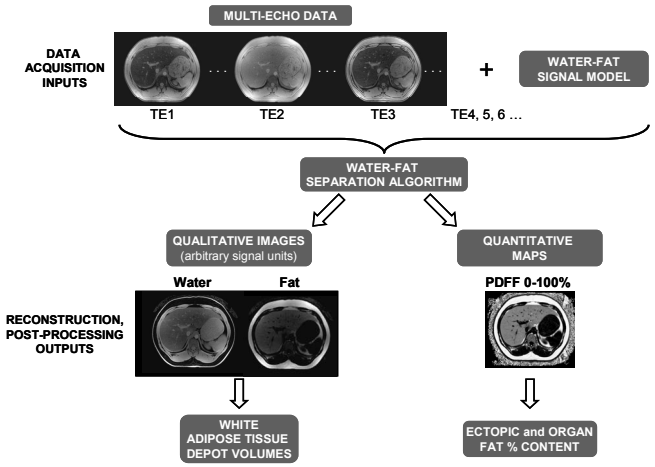

Fig. 7 WFI involves data acquisition of multiple images at strategic echo times to capture the complex water and fat magnetizations at various phase evolutions. Utilizing a signal model that takes into consideration a multi-peak fat spectrum along with other assumptions and constraints, a reconstruction algorithm yields a pair of co-registered water and fat volumes. In parallel, the algorithm generates a PDFF map from 0-100%. The qualitative water-fat data sets are adequate for computing white adipose tissue depot volumes. The PDFF map provides a measure of percent fat content in ectopic depots and organ on a voxel-wise basis.

As illustrated in Fig. 7, a single WFI acquisition yields reconstructed water and fat images that can be used for white adipose tissue depot segmentation, and a PDFF map that allows the measurement of ectopic fat fractions. In Fig. 8, the utility of WFI is demonstrated with clinical data.

VIII. Summary of MR Fat Qunatification

MRI and MRS provide a family of complementary methods for sensitively detecting and quantifying adipose tissue volumes and ectopic fat fractions. T_1-weighted and frequency-selective approaches manipulate and exploit signal intensity differences between fatty and lean tissues and aims to highlight the (desired) fat component's contribution to the net acquired signal versus that of water. In contrast, MRS and WFI strategies exploit fat's unique chemical-shift properties to explicitly separate water and fat signal contributions. It is for this very reason that chemical-shift based methods are appropriate for quantifying diffuse ectopic fat.

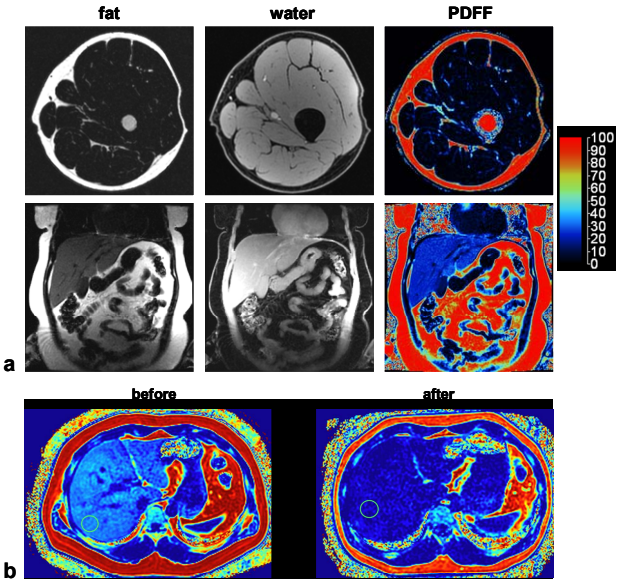

Fig. 8 Examples of WFI are shown in (a) with a transverse section of the thigh (top) and a coronal section (bottom). Reconstructed and co-registered fat, water, and PDFF maps are shown, with the latter on a color scale for visual clarity. (b) WFI in a subject before and after a 10-month exercise and diet regimen. Note the significant loss in subcutaneous and visceral adipose tissue. More evident is the decrease in liver PDFF. Measurements in the liver (green circles) yield a PDFF of 22% before and 6% after exercise and diet intervention.

IX. Image Analysis

Standard procedures for extracting white adipose tissue volumes and ectopic fat signal fractions from data acquired using the aforementioned MR techniques are briefly summarized next. The workflow for extracting fat measures from MR data remains a daunting and costly task in epidemiological studies involving large cohort sizes, and typically requires substantial data post-processing and analysis by a team of experienced operators. The steps typically involve the transfer of images to an offline workstation, followed by the use of home-built or dedicated computer software that require some level of user interaction [82]. While numerous image segmentation algorithms have been developed for gray and white matter extraction from brain images, by comparison, few strategies have been proposed for dedicated utilization in the field of human body composition and fat quantification.

As previously mentioned, for quantification of white adipose tissue depots, a binary signal intensity threshold is commonly applied in conjunction with edge-detection and region-growing strategies and shape-models to T_1-weighted, frequency-selective, and WFI images. The histogram-based threshold is usually applied following a series of steps to correct spatially-varying signal intensities due to bias from non-uniform RF transmit and receiver fields. These corrections are particularly needed for data acquired at 3T and in overweight/obese subjects due to significant dielectric effects. Since fat is characteristically brighter in these data sets, voxels with intensities greater than a set threshold are labeled as white adipose tissue while those with lower intensities are excluded. Many automated algorithms for segmenting subcutaneous and visceral white adipose tissue depots have been proposed [23, 25, 83-86]. For WFI, the analysis can exploit the fat signal fraction map where the signal intensity range is consistently fixed from 0–100% [75].

Automated and semi-automated strategies for ectopic fat quantification are very limited in the literature and have largely only focused on the liver using CT data [87, 88]. Ectopic fat quantification requires approaches that can separate water and fat signals within each voxel, such as MRS, frequency-selective MRI, and WFI. Ectopic fat accumulation is often spatially heterogeneous, and consequently, the aforementioned binary threshold approach of "all fat" or "no fat" voxel classification is inadequate. For MRS, the areas under the water and fat peaks can be calculated with commercial software jMRUI [45] and LCModel [46], which require some user familiarity to obtain decent results. WFI provides a fat signal fraction map across the imaging volume. To determine the fat signal fraction within a particular organ or muscle group, an operator must manually draw regions-of-interest (ROIs). The mean and standard deviation within the ROI is then computed. However, for accurate fat signal fractions, operator care is critical in drawing ROIs and segmenting organs. Equally important is sound knowledge of human anatomy. For example, the pancreas, a small and tortuously-shaped organ, is surrounded by visceral adipose tissues. An inaccurately drawn ROI meant to enclose only the organs may contain erroneous adipose tissue voxels. In such cases, the high fat signal fractions from even a single erroneous adipose tissue voxel will impact the apparent fat signal fraction within the drawn organ ROI.

MR-based fat segmentation remains an active area of research that requires further improvements. Techniques that can automatically segment adipose tissue depots, muscles, and more critically organs (liver, pancreas) while utilizing *a priori* information are being explored with atlas-based algorithms. The capability of achieving rapid fat registration, segmentation, and quantification is highly attractive, and will provide investigators with vital person-specific information reflecting the temporal change in fat distribution and volumes in response to therapeutic interventions.

X. Brown Adipose Tissue, "The Good Fat"

The adipose tissue is considered an organ that is intimately involved in regulating metabolism, energy balance, and fat storage through the secretion of hormones via neural stimulation. Up to this point, one focus of the paper has been on imaging and quantifying white adipose tissue fat storage depots, heretofore referred to as WAT. In mammals, another type of adipose tissue exists, known as brown adipose tissue (BAT), named based on its color appearance in histology. In humans, it has traditionally been believed that BAT exists only during fetal development and disappears shortly after birth, and thus had an insignificant role in human physiology. However, unequivocal findings of BAT in humans with positron emission and computed tomography (PET/CT) in over the past decade, coupled with new evidence from cadaver studies [89], have caused a resurgence of scientific interest in BAT. As illustrated in Fig. 9, one of the most intriguing paradigms of BAT in rodents and potentially now in humans is its involvement in counteracting against WAT fat storage, weight gain, and ultimately the onset of obesity [90-92]. Thus, whereas excess WAT has been linked with many negative health consequences, BAT has been dubbed the "good fat" and is considered a benefit in many aspects of growth and homeostasis. It has also been implicated as a mediator in skeletal muscle and bone development [93, 94]. In humans, the incidence and metabolic activity of BAT and its response to pharmacological agents, temperature, and environment, its relationship to anthropometry and body composition, and its variability due to exercise and diet, all remain in question and are under increasing levels of study.

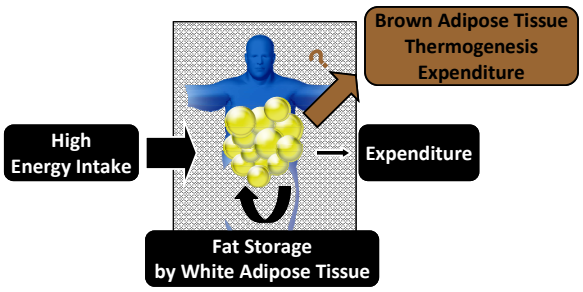

Fig. 9 The role of brown adipose tissue (BAT) in human physiology remains under investigation. When energy intake surpasses baseline metabolic needs, the excess energy is normally channeled into storage as triglycerides in white adipose tissue. It is believed that one of the roles of BAT is to facilitate the expenditure of excess energy from the body via thermogenesis when the tissue is stimulated by the sympathetic nervous system. Thermogenesis thus would counteract white adipose tissue buildup.

WAT and BAT exhibit different morphological features. Whereas WAT is primarily responsible for long-term fat storage, BAT in contrast stores smaller amounts, and instead metabolizes fat to generate heat [95]. While WAT is characterized by large cells that contain a unilocular fat droplet, a displaced peripheral nucleus, and limited cytoplasm water, BAT in contrast contains smaller adipocytes with multiple intracellular fat droplets, a centrally located nucleus, and an abundance of iron-rich mitochondria. These features can be easily recognized with histology [95] and major efforts are now underway to exploit these morphological differences in generating signal contrast mechanisms between BAT and WAT via imaging [96-99]. Furthermore, unlike WAT, BAT is richly vascularized by capillaries that are needed to transport and disperse the produced heat. Currently, MR represents the most promising modality to overcome the limitations and challenges of using PET/CT. Radiation exposure in PET/CT has limited the study of BAT in healthy humans, and this is a highly relevant issue in when involving children, where the prevalence of the tissue is significantly greater than in adults.

The feasibility of using WFI to characterize BAT has been demonstrated in mice and in humans with the fat signal fraction metric. Whereas WAT is predominantly composed of fat and is thus characterized by a high fat signal fraction (>90%), BAT has been shown to occupy a much broader and lower fat signal fraction range. The difference in intracellular iron and mitochondria content and vascular perfusion between BAT and WAT has also led to the utilization of MR techniques that are sensitive to tissue hemodyanmic responses. Investigators have demonstrated an increase in oxygen consumption and consequently greater levels of deoxyhemoglobin in the local blood flow due to BAT activity. The increase in deoxyhemolgobin leads to a decrease in T_2^* [100], resulting in a signal drops that can be observed with blood-oxygen-level-dependent MRI [101, 102].

The further development and validation of sensitive MR techniques to non-invasively quantify BAT is critically needed to advance our knowledge of this tissue in human physiology. Additional distinctive features of BAT have not yet been explored by MRS. For example, BAT's vasculature can be probed by perfusion techniques such as arterial-spin-labeling. Temperature mapping [103] and molecular and metabolic imaging using Carbon-13 are other possibilities. Recent advances in PET/MR also holds promise as an adjunct tool for combined morphological and functional imaging.

XI. Conclusion

In conclusion, MR is the most powerful and comprehensive imaging tool for fat quantification. MR's non-invasive tomographic capability provides insight into the distribution of adipose tissue and fat within the human body that is unmatched by any other modality. Its broad array of sensitive techniques has and will continue to assist investigators to probe fat biomarkers and associations in obesity [104-107].

Acknowledgment

The author thanks the National Institute of Diabetes and Digestive and Kidney Diseases for funding support (K25DK089731). The author acknowledges GE and Philips for technical support at the University of Southern California and Children's Hospital Los Angeles, respectively. The author is grateful for the mentorship of Krishna Nayak, Ph.D., Michael Goran, Ph.D., and Vicente Gilsanz, M.D., Ph.D.

REFERENCES

[1] Ogden CL, Carroll MD, Kit BK, Flegal KM. Prevalence of obesity and trends in body mass index among US children and adolescents, 1999-2010. *JAMA* 2012; 307:483-490.

[2] Flegal KM, Carroll MD, Kit BK, Ogden CL. Prevalence of obesity and trends in the distribution of body mass index among US adults, 1999-2010. *JAMA* 2012; 307:491-497.

[3] Flodmark CE, Lissau I, Moreno LA, Pietrobelli A, Widhalm K. New insights into the field of children and adolescents' obesity: the European perspective. *Int J Obes Relat Metab Disord* 2004; 28:1189-1196.

[4] Zaninotto P, Head J, Stamatakis E, Wardle H, Mindell J. Trends in obesity among adults in England from 1993 to 2004 by age and social class and projections of prevalence to 2012. *J Epidemiol Community Health* 2009; 63:140-146.

[5] Calkins K, Devaskar SU. Fetal origins of adult disease. *Curr Probl Pediatr Adolesc Health Care* 2011; 41:158-176.

[6] Smith SR, Lovejoy JC, Greenway F, Ryan D, deJonge L, de la Bretonne J, Volafova J, Bray GA. Contributions of total body fat, abdominal subcutaneous adipose tissue compartments, and visceral adipose tissue to the metabolic complications of obesity. *Metabolism* 2001; 50:425-435.

[7] Juonala M, Magnussen CG, Berenson GS, et al. Childhood adiposity, adult adiposity, and cardiovascular risk factors. *NEJM* 2011; 365:1876-1885.

[8] Eckel RH, Grundy SM, Zimmet PZ. The metabolic syndrome. *Lancet* 2005; 365:1415-1428.

[9] Grundy SM, Cleeman JI, Daniels SR, Donato KA, Eckel RH, Franklin BA, Gordon DJ, Krauss RM, Savage PJ, Smith Jr SC, Spertus JA, Costa F. Diagnosis and management of the metabolic syndrome. An American Heart Association/National Heart, Lung, and Blood Institute Scientific Statement. Executive summary. *Cardiol Rev* 2005; 13:322-327.

[10] Kuk JL, Katzmarzyk PT, Nichaman MZ, Church TS, Blair SN, Ross R. Visceral fat is an independent predictor of all-cause mortality in men. *Obesity (Silver Spring)* 2006; 14:336-341.

[11] Choudhary AK, Donnelly LF, Racadio JM, Strife JL. Diseases associated with childhood obesity. *Am J Roentgenol* 2007; 188: 1118-1130.

[12] Bergman RN, Kim SP, Hsu IR, Catalano KJ, Chiu JD, Kabir M, Richey JM, Ader M. Abdominal obesity: role in the pathophysiology of metabolic disease and cardiovascular risk. *Am J Med* 2007; 120:S3-8; discussion S29-32.

[13] Demerath EW, Reed D, Rogers N, Sun SS, Lee M, Choh AC, Couch W, Czerwinski SA, Chumlea WC, Siervogel RM, Towne B. Visceral adiposity and its anatomical distribution as predictors of the metabolic syndrome and cardiometabolic risk factor levels. *Am J Clin Nutr* 2008; 88:1263-1271.

[14] Despres JP, Lemieux I, Bergeron J, Pibarot P, Mathieu P, Larose E, Rodes-Cabau J, Bertrand OF, Poirier P. Abdominal obesity and the metabolic syndrome: contribution to global cardiometabolic risk. *Arterioscler Thromb Vasc Biol* 2008; 28: 1039-1049.

[15] Mathieu P, Pibarot P, Larose E, Poirier P, Marette A, Despres JP. Visceral obesity and the heart. *Int J Biochem Cell Biol* 2008; 40:821-836.

[16] de Bazelaire CM, Duhamel GD, Rofsky NM, Alsop DC. MR imaging relaxation times of abdominal and pelvic tissues measured in vivo at 3.0 T: preliminary results. *Radiology* 2004; 230:652-659.

[17] Stanisz GJ, Odrobina EE, Pun J, et al. T1, T2 relaxation and magnetization transfer in tissue at 3T. *Magn Reson Med* 2005; 54:507-512.

[18] Reeder SB, Hu HH, Sirlin CB. Proton density fat-fraction: a standardized MR-based biomarker of tissue fat concentration. *J Magn Reson Imag* 2012; doi:10.1002/jmri.23741.

[19] Ross R, Goodpaster B, Kelley D, Boada F. Magnetic resonance imaging in human body composition research. From quantitative to qualitative tissue measurement. *Ann NY Acad Sci* 2000; 904:12-17.

[20] Machann J, Thamer C, Schnoedt B, et al. Standardized assessment of whole body adipose tissue topography by MRI. *J Magn Reson Imaging* 2005; 21:455-462.

[21] Siegel MJ, Hildebolt CF, Bae KT, Hong C, White NH. Total and intraabdominal fat distribution in preadolescents and adolescents: measurement with MR imaging. *Radiology* 2007; 242:846-856.

[22] Positano V, Gastaldelli A, Sironi AM, Santarelli MF, Lombardi M, Landini L. An accurate and robust method for unsupervised assessment of abdominal fat by MRI. *J Magn Reson Imaging* 2004; 20:684-689.

[23] Demerath EW, Ritter KJ, Couch WA, et al. Validity of a new automated software program for visceral adipose tissue estimation. *Int J Obes (London)* 2007; 31:285-291.

[24] Wurslin C, Machann J, Rempp H, Claussen C, Yang B, Schick F. Topography mapping of whole body adipose tissue using A fully automated and standardized procedure. *J Magn Reson Imaging* 2009; 31:430-439.

[25] Kullberg J, Ahlstrom H, Johansson L, Frimmel H. Automated and reproducible segmentation of visceral and subcutaneous adipose tissue from abdominal MRI. *Int J Obes (London)* 2007; 31:1806-1817.

[26] Machann J, Thamer C, Stefan N, et al. Follow-up whole-body assessment of adipose tissue compartments during a lifestyle intervention in a large cohort at increased risk for type 2 diabetes. *Radiology* 2010; 257:353-363.

[27] Kullberg J, Angelhed JE, Lonn L, et al. Whole-body T1 mapping improves the definition of adipose tissue: consequences for automated image analysis. *J Magn Reson Imaging* 2006; 24:394-401.

[28] Olsen DB, Gideon P, Jeppesen TD, Vissing J. Leg muscle involvement in facioscapulohumeral muscular dystrophy assessed by MRI. *J Neurol* 2006; 253:1437-1441.

[29] Goldfarb JW, Arnold S, Han J. Recent myocardial infarction: assessment with unenhanced T1-weighted MR imaging. *Radiology* 2007; 245:245-250.

[30] Kellman P, Hernando D, Arai AE. Myocardial Fat Imaging. *Curr Cardiovasc Imaging Rep* 2010; 3:83-91.

[31] Brix G, Heiland S, Bellemann ME, Koch T, Lorenz WJ. MR imaging of fat-containing tissues: valuation of two quantitative imaging techniques in comparison with localized proton spectroscopy. *Magn Reson Imaging* 1993; 11:977-991.

[32] Ren J, Dimitrov I, Sherry AD, Malloy CR. Composition of adipose tissue and marrow fat in humans by 1H NMR at 7 Tesla. *J Lipid Res* 2008; 49:2055-2062.

[33] Boesch C, Slotboom J, Hoppeler H, Kreis R. In vivo determination of intra-myocellular lipids in human muscle by means of localized 1H-MR-spectroscopy. *Magn Reson Med* 1997; 37:484-493.

[34] Brechtel K, Jacob S, Machann J, et al. Acquired generalized lipoatrophy (AGL): highly selective MR lipid imaging and localized 1H-MRS. *J Magn Reson Imaging* 2000; 12:306-310.

[35] Kreis R, Bruegger K, Skjelsvik C, et al. Quantitative 1H magnetic resonance spectroscopy of myoglobin de- and reoxygenation in skeletal muscle: reproducibility and effects of location and disease. *Magn Reson Med* 2001; 46:240-248.

[36] Schick F, Machann J, Brechtel K, et al. MRI of muscular fat. *Magn Reson Med* 2002; 47:720-727.
[37] Torriani M, Thomas BJ, Halpern EF, Jensen ME, Rosenthal DI, Palmer WE. Intramyocellular lipid quantification: repeatability with 1H MR spectroscopy. *Radiology* 2005; 236:609-614.
[38] van der Meer RW, Rijzewijk LJ, Diamant M, et al. The ageing male heart: myocardial triglyceride content as independent predictor of diastolic function. *Eur Heart J* 2008; 29:1516-1522.
[39] Lingvay I, Esser V, Legendre JL, et al. Noninvasive quantification of pancreatic fat in humans. *J Clin Endocrinol Metab* 2009; 94:4070-4076.
[40] Weis J, Johansson L, Ortiz-Nieto F, Ahlstrom H. Assessment of lipids in skeletal muscle by high-resolution spectroscopic imaging using fat as the internal standard: Comparison with water referenced spectroscopy. *Magn Reson Med* 2008; 59:1259-1265.
[41] Kim H, Taksali SE, Dufour S, et al. Comparative MR study of hepatic fat quantification using single-voxel proton spectroscopy, two-point dixon and three-point IDEAL. *Magn Reson Med* 2008; 59:521-527.
[42] van der Meer RW, Lamb HJ, Smit JW, de Roos A. MR Imaging Evaluation of Cardiovascular Risk in Metabolic Syndrome. *Radiology* 2012; 264:21-37.
[43] Hamilton G, Yokoo T, Bydder M, et al. In vivo characterization of the liver fat 1H MR spectrum. *NMR Biomed* 2010; 24:784-790.
[44] Van Werven JR, Hoogduin JM, Nederveen AJ, et al. Reproducibility of 3.0 Tesla magnetic resonance spectroscopy for measuring hepatic fat content. *J Magn Reson Imaging* 2009; 30:444-448.
[45] Naressi A, Couturier C, Castang I, de Beer R, Graveron-Demilly D. Java-based graphical user interface for MRUI, a software package for quantitation of in vivo/medical magnetic resonance spectroscopy signals. *Comput Biol Med* 2001; 31:269-286.
[46] Provencher SW. Estimation of metabolite concentrations from localized in vivo proton NMR spectra. *Magn Reson Med* 1993; 30:672-679.
[47] Reeder SB, Cruite I, Hamilton G, Sirlin CB. Quantitative assessment of liver fat with magnetic resonance imaging and spectroscopy. *J Magn Reson Imaging* 2011; 34:729-749.
[48] Schick F, Eismann B, Jung WI, Bongers H, Bunse M, Lutz O. Comparison of localized proton NMR signals of skeletal muscle and fat tissue in vivo: two lipid compartments in muscle tissue. *Magn Reson Med* 1993; 29:158-167
[49] Szczepaniak LS, Dobbins RL, Stein DT, McGarry JD. Bulk magnetic susceptibility effects on the assessment of intra- and extramyocellular lipids in vivo. *Magn Reson Med* 2002; 47:607-610.
[50] Stein DT, Szczepaniak LS, Dobbins R, malloy CR, McGarry JD. Skeletal muscle triglyceride stores are increased in insulin resistance. *Diabetes* 1997; 46-Suppl1:23A.
[51] Krssak M, Petersen KF, Dresner A, DiPietro L, Vogel SM, Rothman DL, Shulman GI, Roden M. Intramyocellular lipid concentrations are correlated with insulin sensitivity in humans: a 1H NMR spectroscopy study. *Diabetologia* 1999; 42:113-116.
[52] Jacob S, Machann J, Rett K, Brechtel K, Volk A, Renn W, Maerker E, Matthaei S, Schick F, Claussen CD, Haring HU. Association of increased intramyocellular lipid content with insulin resistance in lean nondiabetic offspring of type 2 diabetic subjects. *Diabetes* 1999; 48:1113-1119.
[53] Decombaz J, Schmitt B, Ith M, Decarli B, Diem P, Kreis R, Hoppeler H, Boesch C. Postexercise fat intake repletes intramyocellular lipids but no faster in trained than in sedentary subjects. *Am J Physiol Regul Integr Comp Physiol* 2001; 281:R760-769.
[54] Goodpaster BH, He J, Watkins S, Kelley DE. Skeletal muscle lipid content and insulin resistance: evidence for a paradox in endurance-trained athletes. *J Clin Endocrinol Metab* 2001; 86:5755-5761.
[55] Thamer C, Machann J, Bachmann O, Haap M, Dahl D, Wietek B, Tschritter O, Niess A, Brechtel K, Fritsche A, Claussen C, Jacob S, Schick F, Haring HU, Stumvoll M. Intramyocellular lipids: anthropometric determinants and relationships with maximal aerobic capacity and insulin sensitivity. *J Clin Endocrinol Metab* 2003; 88:1785-1791.
[56] Kaldoudi E, Williams SC, Barker GJ, Tofts PS. A chemical shift selective inversion recovery sequence for fat-suppressed MRI: theory and experimental validation. *Magn Reson Imaging* 1993; 11:341-355.
[57] Laurent WM, Bonny JM, Renou JP. Imaging of water and fat fractions in high-field MRI with multiple slice chemical shift-selective inversion recovery. *J Magn Reson Imaging* 2000; 12:488-496.
[58] Machann J, Bachmann OP, Brechtel K, et al. Lipid content in the musculature of the lower leg assessed by fat selective MRI: intra- and inter- individual differences and correlation with anthropometric and metabolic data. *J Magn Reson Imaging* 2003; 17:350-357.
[59] Machann J, Thamer C, Schnoedt B, et al. Hepatic lipid accumulation in healthy subjects: a comparative study using spectral fat-selective MRI and volume-localized 1H-MR spectroscopy. *Magn Reson Med* 2006; 55:913-917.
[60] Peng Q, McColl RW, Ding Y, Wang J, Chia JM, Weatherall PT. Automated method for accurate abdominal fat quantification on water-saturated magnetic resonance images. *J Magn Reson Imaging* 2007; 26:738-746.
[61] Makrogiannis S, Serai S, Fishbein KW, Schreiber C, Ferrucci L, Spencer RG. Automated quantification of muscle and fat in the thigh from water-, fat-, and nonsuppressed MR images. *J Magn Reson Imaging* 2012; 35:1152-1161.
[62] Hood MN, Ho VB, Smirniotopoulos JG, Szumowski J. Chemical shift: the artifact and clinical tool revisited. *Radiographics* 1999; 19:357-371.
[63] Bley TA, Wieben O, Francois CJ, Brittain JH, Reeder SB. Fat and water magnetic resonance imaging. *J Magn Reson Imaging* 2011; 31:4-18.
[64] Ma J. Dixon techniques for water and fat imaging. *J Magn Reson Imaging* 2008; 28:543-558.
[65] Cassidy FH, Yokoo T, Aganovic L, et al. Fatty liver disease: MR imaging techniques for the detection and quantification of liver steatosis. *Radiographics* 2009; 29:231-260.
[66] Dixon WT. Simple proton spectroscopic imaging. *Radiology* 1984; 153:189-194.
[67] Xiang QS. Two-point water-fat imaging with partially-opposed-phase (POP) acquisition: an asymmetric Dixon method. *Magn Reson Med* 2006; 56:572-584.
[68] Eggers H, Brendel B, Duijndam A, Herigault G. Dual-echo Dixon imaging with flexible choice of echo times. *Magn Reson Med* 2011; 65:96-107.
[69] Berglund J, Kullberg J. Three-dimensional water/fat separation and T2* estimation based on whole-image optimization--application in breathhold liver imaging at 1.5 T. *Magn Reson Med* 2011; 67:1684-1693.

[70] Bydder M, Yokoo T, Yu H, Carl M, Reeder SB, Sirlin CB. Constraining the initial phase in water-fat separation. *Magn Reson Imaging* 2011; 29:216-221.
[71] Hernando D, Liang ZP, Kellman P. Chemical shift-based water/fat separation: a comparison of signal models. *Magn Reson Med* 2010; 64:811-822.
[72] Liu CY, McKenzie CA, Yu H, Brittain JH, Reeder SB. Fat quantification with IDEAL gradient echo imaging: correction of bias from T1 and noise. *Magn Reson Med* 2007; 58:354-364.
[73] Bydder M, Yokoo T, Hamilton G, et al. Relaxation effects in the quantification of fat using gradient echo imaging. *Magn Reson Imaging* 2008; 26:347-359.
[74] Hernando D, Hines CD, Yu H, Reeder SB. Addressing phase errors in fat-water imaging using a mixed magnitude/complex fitting method. *Magn Reson Med* 2012; 67:638-644.
[75] Alabousi A, Al-Attar S, Joy TR, Hegele RA, McKenzie CA. Evaluation of adipose tissue volume quantification with IDEAL fat-water separation. *J Magn Reson Imaging* 2011; 34:474-479.
[76] Yokoo T, Shiehmorteza M, Hamilton G, et al. Estimation of hepatic proton-density fat fraction by using MR imaging at 3.0 T. *Radiology* 2011; 258:749-759.
[77] Meisamy S, Hines CD, Hamilton G, et al. Quantification of hepatic steatosis with T1-independent, T2-corrected MR imaging with spectral modeling of fat: blinded comparison with MR spectroscopy. *Radiology* 2011; 258:767-775.
[78] Kang GH, Cruite I, Shiehmorteza M, et al. Reproducibility of MRI-determined proton density fat fraction across two different MR scanner platforms. *J Magn Reson Imaging* 2011; 34:928-934.
[79] Hansen KH, Schroeder ME, Hamilton G, Sirlin CB, Bydder M. Robustness of fat quantification using chemical shift imaging. *Magn Reson Imaging* 2012; 30:151-157.
[80] Kellman P, Hernando D, Shah S, et al. Multiecho Dixon fat and water separation method for detecting fibrofatty infiltration in the myocardium. *Magn Reson Med* 2009; 61:215-221.
[81] Karampinos DC, Baum T, Nardo L, et al. Characterization of the regional distribution of skeletal muscle adipose tissue in type 2 diabetes using chemical shift-based water/fat separation. *J Magn Reson Imaging* 2011; 35:899-907.
[82] Bonekamp S, Ghosh P, Crawford S, et al. Quantitative comparison and evaluation of software packages for assessment of abdominal adipose tissue distribution by magnetic resonance imaging. *Int J Obes (London)* 2008; 32:100-111.
[83] Wilhelm Poll L, Wittsack HJ, Koch JA, et al. A rapid and reliable semiautomated method for measurement of total abdominal fat volumes using magnetic resonance imaging. *Magn Reson Imaging* 2003; 21:631-636.
[84] Positano V, Gastaldelli A, Sironi AM, Santarelli MF, Lombardi M, Landini L. An accurate and robust method for unsupervised assessment of abdominal fat by MRI. *J Magn Reson Imaging* 2004; 20:684-689.
[85] Tang Y, Sharma P, Nelson MD, Simerly R, Moats RA. Automatic abdominal fat assessment in obese mice using a segmental shape model. *J Magn Reson Imaging* 2011; 34:866-873.
[86] Leinhard OD, Johansson A, Rydell J, et al. Quantitative abdominal fat estimation using MRI. In: *19th International Conference on Pattern Recognition* 2008; 19:1-4.
[87] Gao L, Heath DG, Kuszyk BS, Fishman EK. Automatic liver segmentation technique for three-dimensional visualization of CT data. *Radiology* 1996; 201:359-364.
[88] Zayane O, Jouini B, Mahjoub MA. Automatic liver segmentation method in CT images *Can J Image Proc & Comp Vis* 2011; 2:92-95.
[89] Hu HH, Tovar JP, Pavlova Z, Smith ML, Gilsanz V. Unequivocal identification of brown adipose tissue in a human infant. *J Magn Reson Imaging* 2012; 35:938-942.
[90] Seale P, Lazar MA. Brown fat in humans: turning up the heat on obesity. *Diabetes* 2009; 58:1482-1484.
[91] Nedergaard J, Bengtsson T, Cannon B. Three years with adult human brown adipose tissue. *Ann NY Acad Sci* 2010; 1212:E20-36.
[92] Ravussin E, Galgani JE. The implication of brown adipose tissue for humans. *Annu Rev Nutr* 2011; 31:33-47.
[93] Gilsanz V, Chung SA, Jackson H, Dorey FJ, Hu HH. Functional brown adipose tissue is related to muscle volume in children and adolescents. *J Pediatr* 2011; 158:722-726.
[94] Motyl KJ, Rosen CJ. Temperatures rising: brown fat and bone. *Discov Med* 2011; 11:179-185.
[95] Cinti S. The role of brown adipose tissue in human obesity. *Nutr Metab Cardiovasc Dis* 2006; 16:569-574.
[96] Osculati F, Leclercq F, Sbarbati A, Zancanaro C, Cinti S, Antonakis K. Morphological identification of brown adipose tissue by magnetic resonance imaging in the rat. *Eur J Radiol* 1989; 9:112-114.
[97] Hu HH, Chung SA, Nayak KS, Jackson HA, Gilsanz V. Differential computed tomographic attenuation of metabolically active and inactive adipose tissues: preliminary findings. *J Comput Assist Tomogr* 2011; 35:65-71.
[98] Hu HH, Smith DL, Jr., Nayak KS, Goran MI, Nagy TR. Identification of brown adipose tissue in mice with fat-water IDEAL-MRI. *J Magn Reson Imaging* 2010; 31:1195-1202.
[99] Branca RT, Warren WS. In vivo brown adipose tissue detection and characterization using water-lipid intermolecular zero-quantum coherences. *Magn Reson Med* 2011; 65:313-319.
[100] Hu HH, Hines CD, Smith DL, Jr., Reeder SB. Variations in T2* and fat content of murine brown and white adipose tissues by chemical-shift MRI. *Magn Reson Imaging* 2012; 30:323-329.
[101] Khanna A, Branca RT. Detecting brown adipose tissue activity with BOLD MRI in mice. *Magn Reson Med* 2012; in press.
[102] Chen YI, Cypess AM, Sass CA, et al. Anatomical and functional assessment of brown adipose tissue by magnetic resonance imaging. *Obesity (Silver Spring)* 2012; 20:1519-1526.
[103] Todd N, Diakite M, Payne A, Parker DL. Hybrid proton resonance frequency/T1 technique for simultaneous temperature monitoring in adipose and aqueous tissues. *Magn Reson Med* 2012; in press.
[104] Canapari CA, Hoppin AG, Kinane TB, Thomas BJ, Torriani M, Katz ES. Relationship between sleep apnea, fat distribution, and insulin resistance in obese children. *J Clin Sleep Med* 2011; 7:268-273.
[105] Samara A, Ventura EE, Alfadda AA, Goran MI. Use of MRI and CT for fat imaging in children and youth: what have we learned about obesity, fat distribution and metabolic disease risk? *Obes Rev* 2012; in press.
[106] Staiano AE, Katzmarzyk PT. Ethnic and sex differences in body fat and visceral and subcutaneous adiposity in children and adolescents. *Int J Obes (London)* 2012; in press.
[107] Thomas EL, Parkinson JR, Frost GS, et al. The missing risk: MRI and MRS phenotyping of abdominal adiposity and ectopic fat. *Obesity (Silver Spring)* 2012; 20:76-87.